Check for updates

View Article Online
View Journal

Polymer Chemistry

Accepted Manuscript

This article can be cited before page numbers have been issued, to do this please use: A. Kann, A. J. D. Krüger, M. Rose and P. Hausoul, *Polym. Chem.*, 2019, DOI: 10.1039/C9PY01193E.

View Article Online
DOI: 10.1039/C9PY01193E
Journal Name

COMMUNICATION

Grignard Synthesis of Fluorinated Nanoporous Element Organic Frameworks based on the Heteroatoms P, B, Si, Sn and Ge

Received 00th January 20xx,
Accepted 00th January 20xx

DOI: 10.1039/x0xx00000x

www.rsc.org/

Anna Kann[a], Andreas J. D. Krüger[a], Marcus Rose[b] and Peter J. C. Hausoul*[a]

We present the synthesis and characterization of fluorinated polymers based on P, B, Si, Sn and Ge as heteroatoms via Grignard activation. The polymers are microporous with hydrophobic surfaces. The borate-based polymer was successfully applied as solid acid catalyst in the esterification of acetic acid with ethanol.

Recently, porous polymers have attracted considerable attention as highly versatile materials for adsorption, separation and storage of gases, in catalysis, for optoelectronic applications and energy storage.[1–4] Especially, metal-organic frameworks (MOFs) and covalent organic frameworks (COFs) are of interest due to their high surface areas and pore volumes.[5–8] In order to tune the surface polarity, porous ionic organic networks were reported.[9–11] Depending on the desired properties such as porosity, polarity and functionality, these materials can be tailored for their application by varying the organic linker and connector element.[12,13]
The utilization of fluorinated linkers was reported for different MOFs and a COF, showing enhanced properties in terms of stability, hydrophobicity, gas affinity and selectivity in comparison to their non-fluorinated materials.[14–20] In continuation of our work on element organic frameworks (EOFs) with P, Si and Sn as connector elements[21–24], here we present the synthesis and characterization of respective fluorinated porous polymers with P, B, Si, Sn and Ge as heteroatoms. The catalytic application of the borate based polymer as solid acid catalyst was demonstrated in the esterification of acetic acid with ethanol as test reaction.
As the activation of the fluorinated biphenyl linker was not successful neither via lithiation as reported for the non-fluorinated linker[22–25] nor via classical Grignard reaction, a

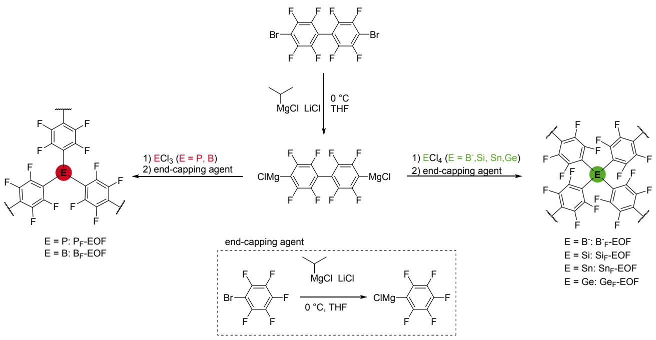

Scheme 1: Synthesis of fluorinated, cross-linked polymers based on various heteroatoms (E_F-EOF (E= P, B, Si, Sn, Ge)).

magnesium-halogen exchange was applied.[26,27] The linker 4,4'-dibromooctafluorbiphenyl was activated twofold with isopropylmagnesium chloride lithium chloride (turbo Grignard) and subsequent reaction with the respective element chlorides in a one-pot procedure (Scheme 1) resulted in the fluorinated polymers E_F-EOF (E= P, B, Si, Sn, Ge). (Perfluorophenyl)-magnesium bromide was used for end-capping, converting remaining E-Cl bonds into E-Ar bonds to form fully substituted trivalent or tetravalent centers, respectively. In all cases, the resulting polymers were obtained as fluffy white powders.
The scanning electron microscopy (SEM) images of all polymers show polydisperse particles, suggesting the

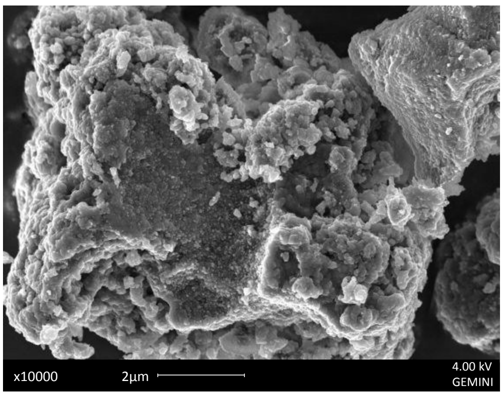

[a] Institut für Technische und Makromolekulare Chemie, RWTH Aachen University, Worringerweg 2, 52074 Aachen, Germany.
E-mail: hausoul@itmc.rwth-aachen.de; Fax: +49 241-80-22177;
Tel: +49 241-80-26561
[b] Technische Chemie II, Technische Universität Darmstadt, Alarich-Weiss-Straße 8, 64287 Darmstadt, Germany.
Electronic Supplementary Information (ESI) available: [details of any supplementary information available should be included here]. See DOI: 10.1039/x0xx00000x

Figure 1: SEM analysis of P_F-EOF with a magnification of 10 000.

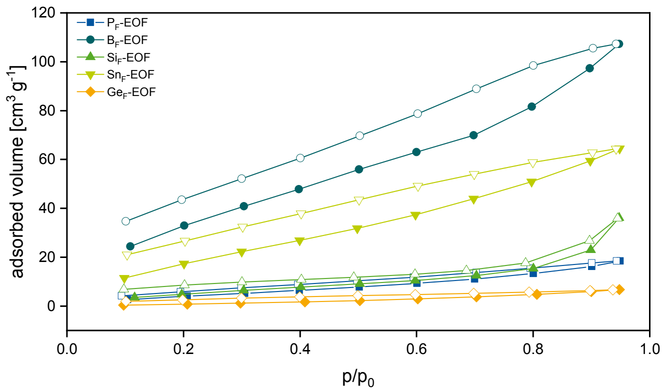

Figure 2: Water vapor physisorption isotherms for fluorinated polymers E_F-EOF (E= P, B, Si, Sn, Ge) measured at 298 K, adsorption with filled symbols, desorption with unfilled symbols.

coalescence of smaller particles (Fig. 1, Fig. S1 in the ESI). Consequently, a broad particle size distribution and relatively undefined particle shapes were found. Energy dispersive X-ray spectroscopy (EDX) analyses of the surfaces showed the presence of C and F with small traces of O in all samples (Figure S2 in the ESI). Additionally, each of the elements P, Sn and Ge were detected in the corresponding polymers, while Si and B were not observed.

View Article Online
DOI: 10.1039/C9PY01193E

All polymers are X-ray diffraction (XRD) amorphous (Fig. S3 in the ESI) and the thermal decomposition (Fig. S4 in the ESI) started between 330 °C and 375 °C, occurring in one or two steps, except for Sn_F-EOF. The Sn-polymer was only stable up to 205 °C and decomposed in three steps. The physical properties are comparable to the ones reported for non-fluorinated polymers based on P[24,28], Si[22] and Sn[23].

Specific surface areas, determined by N_2 physisorption, ranged between 437 – 566 m² g^{-1} (Tab. 1, Tab. S2 in the ESI), whereas trivalent polymers based on P and B exhibited higher surface areas compared to tetravalent materials based on Si, Sn and Ge. In all cases, the external surface areas are relatively high (54 – 65 % of the specific surface area), most probably due to the presence of small particles, as reported in previous publications.[22,23] In comparison to non-fluorinated polymers, a slightly increased specific surface area was realized for P_F-EOF, while the specific surface area of Si_F-EOF was reduced and the one of Sn_F-EOF was similar to the non-fluorinated polymer.[22–25]

The pore size distribution (Fig. S5 in the ESI) confirms the microporous nature of these polymers.

The corresponding isotherms show a combination of type I and II according to the IUPAC classification, typical for element organic frameworks (Fig. 3). The high uptake at low relative pressures indicates the presence of micropores and the hysteresis is extended over the whole range of pressure, most probably due to its flexibility, resulting from the swelling of the amorphous framework.[23]

Table 1: Specific surface areas of synthesized fluorinated polymers E_F-EOF (E= P, B, Si, Sn, Ge) in comparison to the reported values for the non-fluorinated EOFs and chemical composition of these fluorinated polymers: ideal and found in elemental analyses.

E	S_{BET} for E_F-EOF [m² g^{-1}]	S_{BET} for E-EOF [m² g^{-1}]	C [%]		F [%]		E [%]		Total [%]
			Calc.	Found	Calc.	Found	Calc.	Found	
P	538	458 [25]	45.5	44.6	48.0	34.9	6.5	8.7	88.2
B	566	-	47.5	48.8	50.1	41.9	2.4	2.5	93.2
Si	447	1046 [22]	46.5	48.9	49.0	50.1	4.5	0.8	99.8
Sn	437	445 [23]	40.5	39.3	42.8	41.5	16.7	12.6	93.4
Ge	452	-	43.3	46.2	45.7	43.9	11.0	7.7	97.8

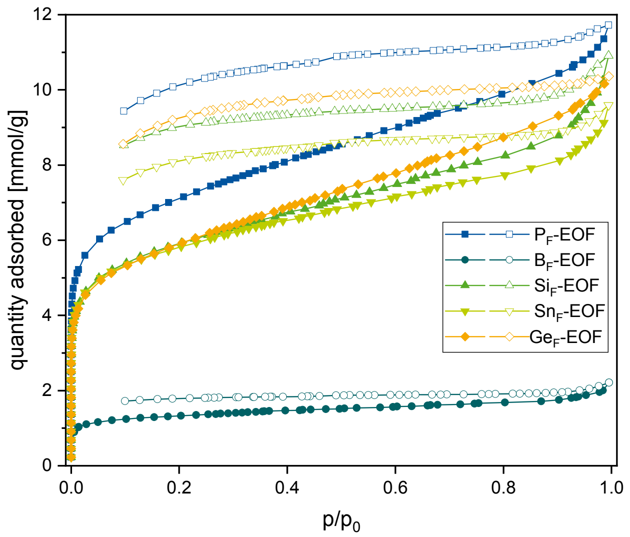

Figure 3: Nitrogen physisorption isotherms for fluorinated polymers E_F-EOF (E= P, B, Si, Sn, Ge) measured at 77 K. Adsorption with filled symbols, desorption with unfilled symbols. E_F-EOF (E= B, Si, Sn, Ge) were offset with +15, +20, +30, +40, respectively.

The utilization of fluorinated biphenyl linkers and a complete cross-linking led to materials with high hydrophobicity, which was confirmed by water vapor physisorption (Fig. 2). In the case of BF-EOF, higher water adsorption is most probably due to the existence of charged BR_4^- species as described later. In relation to commercial adsorbents such as activated carbons or zeolites, the hydrophobic character of fluorinated polymers is clearly increased.

The chemical composition was examined using elemental analysis (EA, Tab. 1). $E(C_6F_4)_3$ (E = P, B) and $E(C_6F_4)_4$ (E = Si, Sn, Ge) were expected as the ideal composition of the polymeric materials. In the case of P_F-EOF, a lower F content and a higher P content were found. For B_F-EOF, the expected content of B was achieved, while the F content was lower. For the tetravalent polymers, the determined composition for C and F are in good agreement with the expected values. However, in all tetravalent polymers the heteroatom content was lower

View Article Online
DOI: 10.1039/C9PY01193E

than expected value. A slight excess of linker in the polymer is expected due to presence of defects at the surface and interior of the polymer. However the low incorporation of Si in the backbone suggest the occurrence of side reactions. One likely possibility is the generation of reactive aryne species via the elimination of adjacent silyl and fluorine groups which in turn react with the linker to poly(perfluorophenyl)oligomers. In effect this reduces the number of crosslinks and could explain why the BET surface area of Si_F-EOF is roughly halved compared to the non-fluorinated analog. The total mass balances varied between 88.2 % and 99.8 %. Mass loss might be due to the incorporation of the respective salts during the synthesis.

The polymer was further characterized by attenuated total reflection infrared spectroscopy (ATR-IR). The spectra show four major bands in all cases (Fig. S6), suggesting similar chemical structures. In addition, X-ray photoelectron spectroscopy (XPS) measurements were performed (Fig. 4, Fig S7-10 in the ESI) and all spectra were referenced to 690.9 eV, corresponding to the aromatic fluorine atom in C_6F_6.[29] The C1s spectra show three overlapping signals corresponding to carbon atoms bond to fluorine in the aromatic ring (290.4-290.6 eV), the carbon atoms of the biphenyl bridge (288.7-288.9 eV) and the carbon atoms bond to the element (287.0-287.3 eV).[30,31] Only for the P containing polymer the binding energy of the carbon atom bond to phosphorous is shifted to 292.6 eV. An additional peak at 291.4-294.8 eV was observed for P, B and Ge containing polymers, most probably due to characteristic $\pi \rightarrow \pi^*$ shake-up peaks for aromatic structures.[32,33] Considering the F1s spectra, the presence of a single sharp peak for fluorine bond to the aromatic ring at 690.9 eV confirms the proposed structure. Only for P and Ge containing polymers, an additional peak at higher binding energies (692.4-693.0 eV) was obtained. For all heteroatoms, characteristic peaks were observed in the survey spectra.

The polymers were further characterized by solid-state nuclear magnetic resonance (NMR) spectroscopy with magic angle

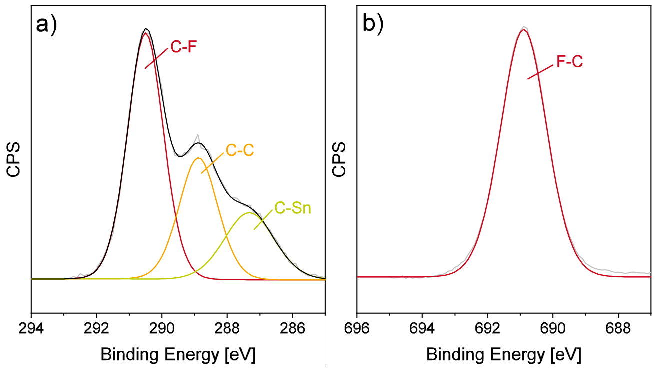

Figure 4: XPS spectra of Sn_F-EOF, a) C 1s und b) F 1s, referenced to F1s at 690.9 eV.

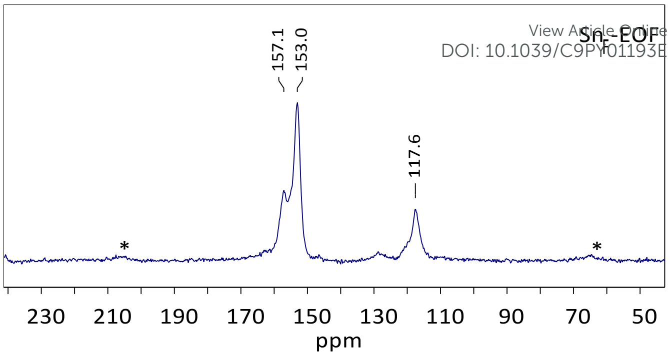

Figure 5: CP from ^{19}F to ^{13}C MAS NMR of Sn_F-EOF.

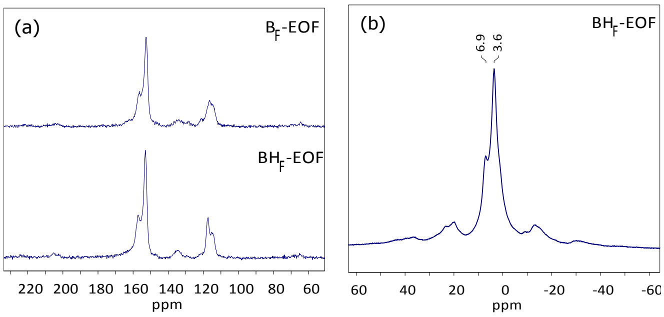

Figure 6: a) CP from ^{19}F to ^{13}C MAS NMR of B_F-EOF before and BH_F-EOF after the treatment with HCl (11 kHz), b) ^{1}H MAS NMR of BH_F-EOF (11 kHz).

spinning (MAS). Cross polarization (CP) from ^{19}F to ^{13}C MAS NMR confirmed the proposed polymer structures as the peaks at 157.2-153.0 ppm correspond to the C-C and C-F bonds, the peaks at 121.2-115.2 ppm to the C-E bond (Fig. 5, Fig S11 in the ESI). In ^{19}F MAS NMR, the presence of fluorine in the polymer was identified, showing similar peaks for all polymers and comparable spectra to the linker 4,4'-dibromooctafluorbiphenyl (Fig S12 in the ESI).

In addition, $^{31}P\{^{19}F\}$ MAS NMR was performed for P_F-EOF (Fig. S13 in the ESI), showing an intense single peak at -79.0 ppm, which suggests complete cross-linking to PR_3.[34–36] Phosphorus oxides were not observed. The $^{119}Sn\{^{19}F\}$ MAS NMR of Sn_F-EOF presents a peak at -243.3 ppm (Fig. S14 in the ESI), which is in agreement with molecular $Sn(C_6F_5)_4$.[37] In $^{11}B\{^{19}F\}$ MAS NMR of B_F-EOF, peaks at 18.4 and -5.22 ppm were observed (Fig. S15 in the ESI). This reveals the appearance of different boron species. Boranes (BR_3, $R=C_6F_4$) were not formed, as a chemical shift around 60 ppm was not observed.[38,39] The peak at -5.22 ppm most probably corresponds to borate species of BR_4^- and BR_3OH^-, as chemical shifts of -17 ppm to -2.7 ppm were reported.[9,39–42] The peak at 18.4 ppm and an additional shoulder at lower chemical shifts were likely assigned to $BR_3(OMe)$ and $BR_2(OMe)_2$, as peaks at 2.0 to 26.1 ppm were reported in literature for these species.[43,44] These species can be formed due to incomplete polymerization and quenching with methanol.

Due to the presence of borate species, an cation exchange was performed with hydrochloric acid in order to obtain a solid acid catalyst in the type of $B^-H^+{}_F$-EOF. The material was characterized by CP from ^{19}F to ^{13}C, ^{19}F and $^{11}B\{^{19}F\}$ MAS NMR, showing no change of the polymer structure during the ion-exchange (Fig. 6a, Fig. S16-S17 in the ESI). In addition, the presence of protons in the polymer was confirmed by ^{1}H MAS NMR, showing peaks at 6.9 and 3.6 ppm (Fig. 6b).

The catalytic performance of BH_F-EOF as solid acid catalyst was tested in the esterification of acetic acid (AcOH) with ethanol (EtOH) to ethyl acetate (AcOEt). Our catalyst was compared to commercial Amberlyst 15 hydrogen form, a cation exchange resin, and Nafion NR50, a perfluorinated polymer with SO_3H groups. The amount of acidic sites for each catalyst was determined by Boehm Titration.[45] Here, Amberlyst 15 H form had the highest proton density with 5.22 mmol H^+/ $g_{catalyst}$. Nafion NR50 (1.48 mmol H^+/ $g_{catalyst}$) and BH_F-EOF

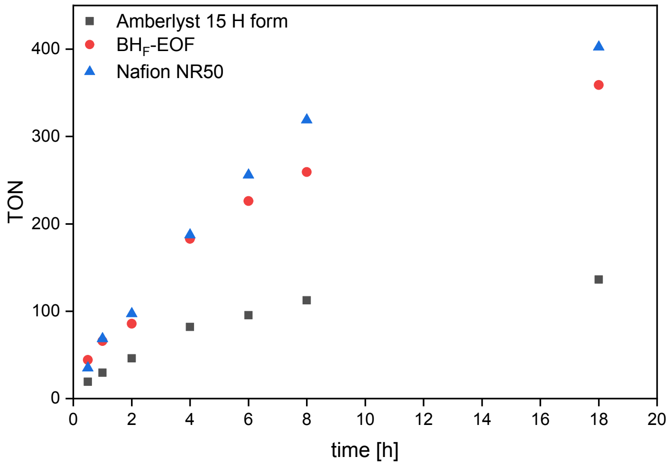

Figure 7: Esterification of acetic acid with ethanol to ethyl acetate. Catalysts: Amberlyst 15 hydrogen form (grey), BH_F-EOF (red) and Nafion NR 50 (blue). Conditions: 60 °C, 34.6 mmol EtOH and AcOH, 30 mg catalyst. TON = mol_{AcOEt} pro mol_{H+}.

(1.30 mmol H^+/ $g_{catalyst}$) showed a lower but comparable number of acidic sites. The esterification of AcOH with EtOH was performed in pressure-tubes at 60 °C for different time intervals (Fig. 7). The yield of AcOEt was referred to the quantity of acidic sites, expressed as turnover number (TON). In addition, the initial turnover frequency (TOF) was determined after 30 minutes, in order to compare the activity of the different catalysts. Our catalyst BH_F-EOF was identified as the most active catalyst with an initial TOF of 88 h^{-1} and a maximum TON of 359 after 18 h. With a slightly lower initial TOF of 70 h^{-1}, Nafion NR50 showed comparable activity in the esterification with a maximum TON of 402. The Amberlyst 15 hydrogen form presented the lowest activity with an initial TOF of only 39 h^{-1} and a TON of 136 after 18 h. With these experiments, we could confirm the applicability of BH_F-EOF as solid acid catalyst in a typical acid-catalyzed reaction with a high activity, which is comparable to commercially used solid acids.

Conclusions

In summary, we presented the successful cross-linking of the fluorinated linker 4,4'-dibromooctafluorbiphenyl with element chlorides based on P, B, Si, Sn and Ge as connector elements. The resulting polymers are amorphous and microporous with specific surface areas of 437-566 $m^2\ g^{-1}$, showing a high hydrophobicity and thermal stability. Investigations on the chemical structure by MAS NMR, XPS, IR and EA confirmed the proposed structures. Only the trivalent structure of the B based polymer was not formed, instead borate species were observed. An ion-exchange of this material with hydrochloric acid obtained a solid acid catalyst which was successfully applied in the heterogeneously catalyzed esterification of acetic acid with ethanol. The material presents a high activity and productivity compared to commercially available solid acids.

View Article Online
DOI: 10.1039/C9PY01133J

Conflicts of interest

There are no conflicts to declare.

Acknowledgement

We gratefully acknowledge financial support by the German Research Foundation, Grant No. RO 4757/2-1 for the Grignard route to Element Organic Frameworks and RO 4757/5-1 for the use of fluorinated Linkers in EOFs. A.K. thanks the German Federal Environmental Foundation for financial support. We thank Karl-Josef Vaeßen for TG, XRD and N_2 physisorption, and Elke Biener and Hannelore Eschmann for GC analyses.

Notes and references

1 N. Chaoui, M. Trunk, R. Dawson, J. Schmidt and A. Thomas, Chem. Soc. Rev., 2017, 46, 3302–3321.
2 A. G. Slater and A. I. Cooper, Science, 2015, 348, aaa8075-aaa8075.
3 L. Tan and B. Tan, Chem. Soc. Rev., 2017, 46, 3322–3356.
4 A. Thomas, Angew. Chem. Int. Ed., 2010, 49, 8328–8344.
5 S. B. Alahakoon, C. M. Thompson, G. Occhialini and R. A. Smaldone, ChemSusChem, 2017, 10, 2116–2129.
6 R. P. Bisbey and W. R. Dichtel, ACS Cent. Sci., 2017, 3, 533–543.
7 J. Jiang, Y. Zhao and O. M. Yaghi, J. Am. Chem. Soc., 2016, 138, 3255–3265.
8 O. Yahiaoui, A. N. Fitch, F. Hoffmann, M. Fröba, A. Thomas and J. Roeser, J. Am. Chem. Soc., 2018, 140, 5330–5333.
9 S. Fischer, J. Schmidt, P. Strauch and A. Thomas, Angew. Chem. Int. Ed., 2013, 52, 12174–12178.
10 J. Roeser, D. Prill, M. J. Bojdys, P. Fayon, A. Trewin, A. N. Fitch, M. U. Schmidt and A. Thomas, Nat. Chem., 2017, 9, 977–982.
11 J.-K. Sun, M. Antonietti and J. Yuan, Chem. Soc. Rev., 2016, 45, 6627–6656.
12 M. Rose, ChemCatChem, 2014, 6, 1166–1682.
13 A. Nagai, Z. Guo, X. Feng, S. Jin, X. Chen, X. Ding and D. Jiang, Nat. Commun., 2011, 2, 536–538.
14 M. Pagliaro and R. Ciriminna, J. Mater. Chem., 2005, 15, 4981–4991.
15 A. P. Kharitonov, J. Fluor. Chem., 2000, 103, 123–127.
16 Z. Hulvey, D. A. Sava, J. Eckert and A. K. Cheetham, Inorg. Chem., 2011, 50, 403–405.
17 C. Yang, U. Kaipa, Q. Z. Mather, X. Wang, V. Nesterov, A. F. Venero and M. A. Omary, J. Am. Chem. Soc., 2011, 133, 18094–18097.
18 C. Serre, Angew. Chem. Int. Ed., 2012, 51, 6048–6050.
19 C. Yang, X. Wang and M. A. Omary, J. Am. Chem. Soc., 2007, 129, 15454–15455.

View Article Online
DOI: 10.1039/C9PY01193E

20 T. H. Chen, I. Popov, O. Zenasni, O. Daugulis and O. Š. Miljanić, Chem. Commun., 2013, 49, 6846–6848.
21 M. Rose, N. Klein, W. Böhlmann, B. Böhringer, S. Fichtner and S. Kaskel, Soft Matter, 2010, 6, 3918–3923.
22 M. Rose, W. Böhlmann, M. Sabo and S. Kaskel, Chem. Commun., 2008, 1, 2462–2464.
23 J. Fritsch, M. Rose, P. Wollmann, W. Böhlmann and S. Kaskel, Materials (Basel)., 2010, 3, 2447–2462.
24 P. J. C. Hausoul, T. M. Eggenhuisen, D. Nand, M. Baldus, B. M. Weckhuysen, R. J. M. Klein Gebbink and P. C. A. Bruijnincx, Catal. Sci. Technol., 2013, 3, 2571–2579.
25 J. Fritsch, F. Drache, G. Nickerl, W. Böhlmann and S. Kaskel, Microporous Mesoporous Mater., 2013, 172, 167–173.
26 C. Tamborski and G. J. Moore, J. Organomet. Chem., 1971, 26, 153–156.
27 A. Budinská, J. Václavík, V. Matoušek and P. Beier, Org. Lett., 2016, 18, 5844–5847.
28 J. Fritsch, F. Drache, G. Nickerl, W. Böhlmann and S. Kaskel, Microporous Mesoporous Mater., 2013, 172, 167–173.
29 C. D. Wagner, The Nist X-Ray Photoelctron Spectroscopy (XPS) Database, 1991.
30 G. H. Yang, S. W. Oh, E. T. Kang and K. G. Neoh, J. Vac. Sci. Technol. A, 2002, 20, 1955–1963.
31 S. H. Yang, C. H. Liu, W. T. Hsu and H. Chen, Surf. Coatings Technol., 2009, 203, 1379–1383.
32 A. Morais, J. P. C. Alves, F. A. S. Lima, M. Lira-Cantu and A. F. Nogueira, J. Photonics Energy, 2015, 5, 057408-1-057408-21.
33 K. Dave, K. H. Park and M. Dhayal, RSC Adv., 2015, 5, 107348–107354.
34 M. Reißmann, A. Schäfer, S. Jung and T. Müller, Organometallics, 2013, 32, 6736–6744.
35 O. J. Metters, S. J. K. Forrest, H. A. Sparkes, I. Manners and D. F. Wass, J. Am. Chem. Soc., 2016, 138, 1994–2003.
36 A. Schäfer, M. Reißmann, A. Schäfer, W. Saak, D. Haase and T. Müller, Angew. Chem. Int. Ed., 2011, 50, 12636–12638.
37 I.-M. Ramirez y Medina, M. Rohdenburg, F. Mostaghimi, S. Grabowsky, P. Swiderek, J. Beckmann, J. Hoffmann, V. Dorcet, M. Hissler and A. Staubitz, Inorg. Chem., 2018, 57, 12562–12575.
38 K. Bläsing, J. Bresien, R. Labbow, A. Schulz and A. Villinger, Angew. Chem. Int. Ed., 2018, 57, 9170–9175.
39 V. Varga, M. Lamač, M. Horáček, R. Gyepes and J. Pinkas, Dalt. Trans., 2016, 45, 10146–10150.
40 O. J. Metters, S. R. Flynn, C. K. Dowds, H. A. Sparkes, I. Manners and D. F. Wass, ACS Catal., 2016, 6, 6601–6611.
41 V. Fasano and M. J. Ingleson, Chem. - A Eur. J., 2017, 23, 2217–2224.
42 A. R. Siedle, R. A. Newmark and W. M. Lamanna, Organometallics, 1993, 12, 1491–1492.
43 N. Yu, V. V Bardin, U. Flörke and H. Frohn, Z. Anorg. Allg. Chem., 2005, 631, 2638–2646.
44 N. Y. Adonin and V. V Bardin, Russ. Chem. Rev., 2010, 79, 757–785.
45 I. Delidovich and R. Palkovits, Microporous Mesoporous Mater., 2016, 219, 317–319.

View Article Online
DOI: 10.1039/C9PY01193E